XIII. Liquid Propulsion

PROPULSION DIVISION

A. Reaction Control Gas Supply System,

T. A. Groudle

1. Introduction

Experiments relative to the use of neat hydrazine as a monopropellant fuel to generate gases for an attitude control system for unmanned space missions (warm gas attitude control system) were discussed in SPS 37-36, Vol. IV, p. 50, and SPS 37-37, Vol. IV, p. 159. Now, an additional series of tests have been performed to define the problems of large numbers of pulses (i.e., several days of intermittent pulsing), and to investigate filter contamination from generator by-products.

2. Pulse Mode Test

The method used for testing the 0.5 lb_f equivalent thrust gas generator system is shown in Fig. 1. Several firing tests were performed with this configuration to establish such basic performance parameters as chamber pressure and chamber temperature. The gas generator was essentially off-the-shelf hardware, and, more importantly, it was originally designed as a thruster using hydrazine-hydrazine nitrate as the propellant. The performance of this generator with neat hydrazine, however, was adequate for the purposes of this preliminary system. The chamber pressure (p_c) was nominally 90 to 110 psig, the flow rate ($\dot{w}$) was 0.0041 lb_m/sec, and the chamber temperature (T_c) was 1545°F. These measurements were at steady-state conditions (~30 sec firing time), and were degraded considerably during pulse mode operation (p_c = 50 to 80 psig; T_c = 1000 to 1500°F; $\dot{w}$ = 0.003 lb_m/sec).

The gas generator system was connected to a *Ranger*-type attitude control thruster system (Fig. 2) through a 9-μ mechanical labyrinth filter of JPL design, and a 2-μ Millipore[1] mechanical filter. A firing of this combined system was performed for 30 continuous pulses, with an average pulse length of 30 msec. Two attitude control system (ACS) thrusters were cycled such that one thruster was continuously on, and the other operated at random intervals. The warm gas system (WGS) maintained a pressure of 15$^{+0}_{-2}$ psig during the test, and met the demand of the ACS.

[1]Millipore Corp., Bedford, Massachusetts.

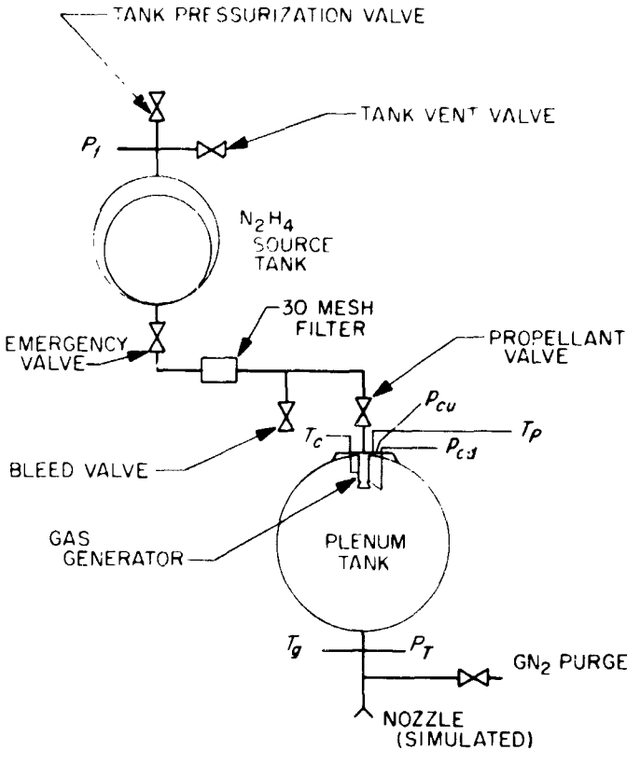

T_P MOUNTING PLATE TEMPERATURE
P_f FUEL TANK PRESSURE
T_c GENERATOR CHAMBER TEMPERATURE
T_g GAS TEMPERATURE
P_{cd} GENERATOR CHAMBER PRESSURE (DOWNSTREAM)
P_{cu} GENERATOR CHAMBER PRESSURE (UPSTREAM)
P_T PLENUM TANK PRESSURE

Fig. 1. Warm gas system schematic

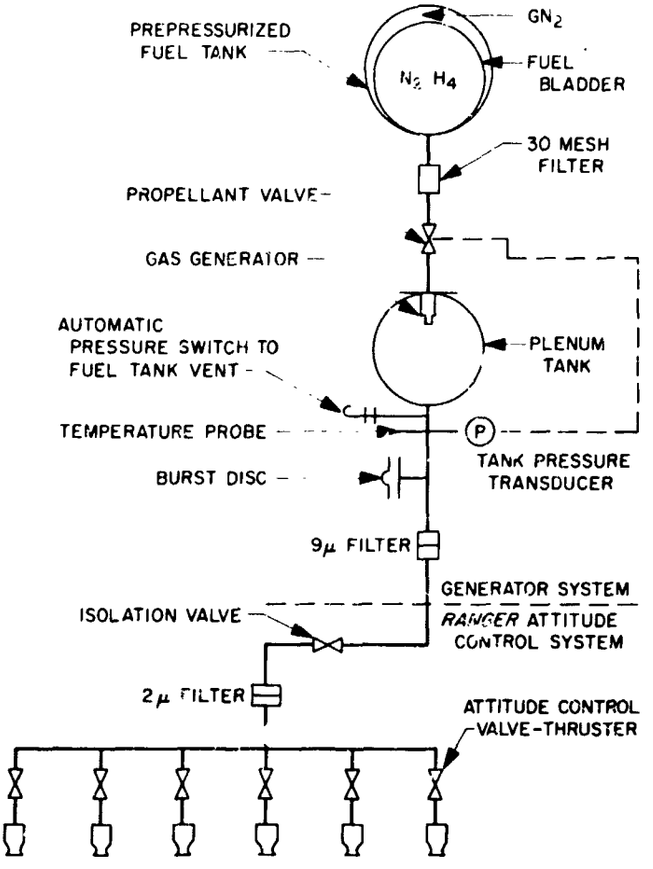

Fig. 2. Warm gas attitude control system schematic

An examination of the filters was made at the end of this test firing. The 9-μ filter was quite dirty with particles from 8 μ to 250 μ in diameter, which appeared to be catalyst fines from the gas generator packed bed. The 2-μ filter was very clean with only a few 2-μ to 3-μ particles.

The 2-μ filter was recleaned; a new 5-μ mechanical filter[2] was installed in place of the 9-μ filter while the latter was being cleaned. A WGS firing of 50 pulses (pulse duration$_{(avg.)}$ = 100 msec) with 3 ACS valves open was performed. The combined system worked very well, with the WGS meeting the ACS demand on the plenum tank. Table 1 describes the recorded performance of the WGS parameters. At the termination of this test, the filters were again examined. The 5-μ filter had trapped several metallic and non-metalic particles from 1 to 100 μ, and one 520-μ particle. A green residue of crystalline structure was also found in the filter; a chemical analysis indicated that the green substance was inorganic. Logically, it was formed as a result of an electrolytic couple of aluminum and stainless steel in the system. These ingredients, in the presence of moisture, ammonia, and traces of hydrazine, form a good battery. The 2-μ Millipore filter was not discolored, and only a few 5-μ particles were present. This is interesting because the Millipore-type filter was expected to produce more of the "green" contamination.

The test was repeated using a clean 2-μ filter and a Vacco[3] 5-μ filter in place of the Permanent filter. Post-test examination revealed that the Millipore filter was slightly dirty (4-μ to 2-μ particles) but had no "green"

[2]Permanent Filter Corp., Compton, California.

[3]Vacco Valve Co., El Monte, California.

Table 1. Results of filter test firing conditions: pulse mode (including pulse no. 1)

Measurement	Value
p_{cd}	87.0 psig (avg.)
P_f	214.5 psig
P_1	13.1 to 15.C psig
p_{cu}	129.0 psig (avg.)
T_c	1547°F (avg.)
T_p	96°F (avg.); 120°F (max.)
T_a	97°F (avg.); 104°F (max.)

contamination The Vacco filter had both non-metallic and metallic particles 1 μ to 60 μ. No "green" contamination was present.

3. Long-Duration Test

It appeared at this time that the contaminants generated by the WGS could be filtered out; it would be desirable, therefore, to run the combined warm gas attitude control system (WGACS) for a cycling test of long duration, based on a *Voyager* condensed mission profile. In preparation for this test, both the WGS and ACS were disassembled and inspected. The WGS had an external green deposit on the generator chamber flange, and the bottom of the plenum tank near the outlet had a uniform coat of loose catalyst dust on the surface. The pressure transducers were removed, and the ⅛ in. pressure tube on the upstream chamber pressure (p_{cu}) was found partially plugged. Small orifices throughout the system are particularly vulnerable to obstruction.

Examination of the ACS revealed a deposit on the thruster valve seats and pintle. A chemical analysis indicated that the deposit was organic. A possible source of the organic material was found on the WGS: a circle of black paint applied to the bottom of the generator mounting plate prior to assembly had not been found in pre-assembly cleaning.

Under operating conditions, a new Eckel[4] propellant valve was cycled with water to provide an indication of how the valve would withstand 4000 cycles of operation. At the end of this test, there were no leaks in the valve and it appeared to operate properly.

Because part of the WGS concept was a "blowdown" method of fuel feed, the level of fuel tank pressurization was calculated to be approximately 1000 psig. However, because a suitable tank could not be readily obtained, a modified *Mariner* Mars 1964 fuel tank was used with a propellant bladder installed. This tank was not designed for pressures greater than 400 psig, and required remote replenishment at selected intervals.

[4]Eckel Valve Co., San Fernando, California.

Table 2. Long-duration test parameters

Measurements	
T_c	Gas generator wall temperature
T_a	Gas temperature
P_f	Fuel tank pressure
p_{cd}	Generator chamber pressure (downstream)
p_{cu}	Generator chamber pressure (upstream)
P_1	Plenum tank pressure
Functions (remote operation)	
ACS thruster valve cycling	
Fuel vent valve	
Fuel line emergency valve	
Plenum tank vent valve	
Generator propellant valve	
Stop/start over-ride switch	

The entire system was reassembled and a test firing was conducted to check the total system and to make a final evaluation of the 9-μ labyrinth and 2-μ mechanical filters. This firing was of 30 min total duration at a pulse rate of 600 msec on, and 2.0 sec off. After this test, the 2-μ filter was examined and found to have several small particles (~3 to 5μ) and the 9-μ filter had fifty to sixty 10- to 30-μ particles. The particles in both filters were of metallic and non-metallic origin. The 2-μ filter element also had a colorless stain and appeared wet. This level of filter contamination was judged acceptable.

The first long-duration mission simulation operation on the WGACS was so conducted that the 21.5 lb_m load of hydrazine in the fuel tank was initially pressurized to 400 psig, and permitted to blow down to 200 psig before repressurization. The system was installed in a protective barricade, and parameter measurements were brought out through an access port. Table 2 lists the parameters monitored. These measurements were recorded on strip charts running at slow speed, and cycled 1 min on every 5 min.

The ACS thruster cycles began according to the sequence in Table 3. The propellant valve was armed, and control was given to the automatic pressure switch (modified pressure transducer). The system operated normally for 10 hr (368 generator pulses) before an electromechanical relay in the pressure switch amplifier failed, causing the gas generator to remain on, and thus creating an overpressure in the plenum tank. At this time both

Table 3. ACS thruster sequence chart

Simulated operation	Thruster response
Separation rate removal, and solar reference acquisition	Open 3 valves for 20 min continuously
Cruise mode	Oper 1 valve every 3.3 sec for 60 msec for 8 days
Commanded turn	Open 3 valves for 5 min
Cruise mode	Open 1 valve every 3.3 sec for 60 msec for 8 days
Commanded turn	Open 3 valves for 5 min
Cruise	Open 1 valve every 3.3 sec for 60 msec for 8 days
Commanded turn	Open 3 valves for 5 min
Cruise	Open 1 valve every 3.3 sec for 60 msec for 8 days
Orbital insertion maneuver	Open 6 valves for 165 min
Cruise	Open 1 valve every 3.3 sec for 60 msec for 8 days

safety devices[5] in the system were activated and the test was terminated.

After repairs to the amplifier circuit and replacement of the burst disk, a second long-duration mission simulation operation was initiated using the same ACS sequence of events. This time, the system operated for 15 hr before automatic shutoff terminated the test; no obvious mechanical failure could be found for this overpressure in the plenum tank.

Subsequently, the expected thrust levels in the ACS thruster changed, creating a need for a larger gas generator to meet the demand. As a result, an off-the-shelf 5.0 lb_f equivalent thrust gas generator was modified to incorporate a "shower head" injector for use with the Shell 405 catalyst[6]. This generator was tested independently and modified until its performance was acceptable for this system. It was not, however, optimized for use as a gas generator (i.e., NH_3 dissociation was still ~50%). The plenum tank was rebuilt to permit installation of this larger generator, and several test-stand firings were made. This generator had been originally designed for neat hydrazine, and its steady-state performance was much smoother than the original, smaller unit. The cold-bed ignition delay time[7] was considerably better as well: 89 msec vs 150 msec for the smaller unit.

The WGACS was reassembled using the larger gas generator and the modified pressure transducer was replaced with a pressure switch[5] to control the pressure in the plenum tank. A new test plan was devised utilizing the same sequence of ACS operation listed in Table 3, except that the cruise mode durations were reduced to provide a 20-day continuous test.

In the third WGACS long-duration test, the system operated continuously for 8 days without disturbance until the burst disk in the plenum tank failed, whereupon the generator operated until all the fuel was depleted. The failed burst disk was examined and found to have been chemically attacked (etched), and, being a thin, aluminum membrane originally (~0.005 in.), the disk had weakened to the point of failure. The electrolytic action that occurred earlier in the filters apparently had appeared again, this time on the disk. The performance of the WGACS from this test is presented in Table 4.

The WGACS was disassembled and examined. The filters had a very large quantity of particulate matter in each element, and both had been severely attacked chemically. Otherwise, the WGS was normal and appeared unaffected by the test. The internal surfaces of the ACS thruster manifolds, however, were heavily spotted with a light brown stain, and the thruster valve seats and ball plunger were coated with a light brown crystalline residue. Corrosion was apparent throughout the ACS components.

A post-test firing was made to provide a gas sample from the plenum tank. The gas was collected by an

[5]The burst pressure of a burst disk on the plenum tank was set at 30 psig; a pressure switch on the plenum tank was set to vent the fuel tank when pressure exceeded 27 psig.

[6]Shell Development Corp., Emeryville, California.

[7]Delay time is measured from propellant valve open to p_c rise.

[8]Custom Component Switches Inc., Burbank, California.

Table 4. Results of 8-day test

Measurement	Value
P_T	17.8 psig (max.) 13.6 psig (min.) (Nominal = $15.0^{+1.8}_{-1.8}$ psig) 15.8 psig (ave.)
P_f	2.5 psig/min (ave.) decay
p_{ca}	80 psig (ave.)
p_{cd}	60 psig (ave.)
Total generator cycles	1695
T_g	75°F (ave.)
T_c	560°F (ave.)

evacuated glass ampul with a remote valve on the end, which was connected to the tee of the plenum tank outlet. One second after ignition, the remote valve was opened for 2 sec and then closed. The ampul was removed and the gas sample analyzed. The general equation for the decomposition of hydrazine is

$$3N_2H_4 \rightarrow 4(1-x)NH_3 + (1+2x)N_2 + 6xH_2$$

where x = the mole fraction of NH_3 dissociated. Assuming 50% NH_3 dissociation, the following results, expressed in mol%, would be expected:

$$NH_3 = 28.6\%$$

$$N_2 = 28.6\%$$

$$H_2 = 42.8\%$$

The results of the analysis, expressed in mol%, follow:

H_2	Ar	O_2	N_2	NH_3	H_2O	C_n	Isopropyl alcohol
37.16	0.32	0.35	37.03	23.62	1.07	0.41	0.04

Argon is expected in the analysis because an argon backfill is used to isolate nitrogen in the analysis of the products. Isopropyl alcohol was present because most of the WGS components were cleaned with this liquid. It appears that a large amount of water formed with some hydrazine in solution. This would indicate inefficient operation of the generator during such short pulses. Most likely, the water is the result of initially-admitted trace amounts of fuel that passed through the catalyst bed without reacting; the fuel normally contains from 1 to 2% water. After several hundred cycles, these trace amounts eventually accumulated into a sizable quantity.

4. Conclusion

The feasibility of the hydrazine plenum warm gas attitude control system was demonstrated by the use of breadboard-type hardware. The test program was hampered by support equipment failures. Several important system problem areas were identified, primarily in the areas of particulate and liquid contamination of the gas, and materials compatibility. No serious or unsolvable problems were encountered. A careful design, with appropriate provision for filtering the gases, should prove highly successful.

B. Liquid Propulsion Systems, *L. R. Toth and O. F. Keller*

1. Introduction, *L. R. Toth*

The Advanced Liquid Propulsion Systems program is investigating selected problems generated by spacecraft operational requirements for propulsion systems capable of high inherent reliability, long-term storage in the space environment, multiple start in free fall (zero gravity), and engine throttling. The proposed solutions to these problems are coordinated for integration into a system.

Beginning with SPS 37-8, Vol. IV, periodic reports describe the progress of work on the various parts of a specific system. Recent advances in material compatibility and bladder development include:

(1) Material compatibility with hydrazine and hydrazine/hydrazine nitrate mix propellants.

(2) Heat sterilization of ethylene-propylene elastomeric material with hydrazine.

2. Material Compatibility, *L. R. Toth*

A number of spacecraft construction materials are subjected to long term compatibility tests in hydrazine (N_2H_4), hydrazine/hydrazine nitrate mix (75% N_2H_4, 24% $N_2H_5NO_3$, 1% H_2O), and nitrogen tetroxide (N_2O_4) propellants.

Each material sample is sealed in a glass ampul; a lox-cleaned pressure gage is attached to permit termination of the test if the internal pressure buildup from decomposition reaches 40 psia. This predetermined cutoff point would preclude failure of the glass ampul. Prior to use, the sealed ampuls are stored at $110 \pm 5°F$ in the material compatibility test facility located at the Edwards Test Station.

Metal specimens are cylinders ¼-in. in diameter and 3 in. long; they are half-immersed in 20 cm^3 of liquid propellant. The elastomeric specimens are typically thin sheets ½ in. wide, 4¾ in. long and 0.03 to 0.06 thick; these are fully immersed in 40 cm^3 of propellant.

All test and specimen data have been fully documented for comparison with post-test analyses. This includes such pertinent controlling information as fixture internal geometry and volume, coding, material physical measurements and properties, propellant composition and volume, and the cleaning procedures involved during preparation. The evaluation of results includes analysis for propellant decomposition, metallurgical analysis to determine the

effects of exposure on the basic material at the liquid interface, and the significance of pitting that results from material constituents. Permeation rates are measured for elastomeric specimens. Complete information will be included in a formal report to be released at the conclusion of this Phase I test program.

The following summarizes the results of tests in progress, and tests that were terminated, but not reported previously.

(1) The status and results for the hydrazine propellant test are summarized in Table 5.

(2) The status and results for the hydrazine/hydrazine nitrate mix propellant test are summarized in Table 6.

(3) The nitrogen tetroxide propellant Phase I testing was concluded on February 1, 1967. A total of forty-four test capsules and specimens of the overall program remained at this point. The complete lot is being subjected to post-test analysis and evaluation, and will be reported at a later date. It is noted that throughout this nitrogen tetroxide Phase I testing, there was no indication of an internal pressure build up.

Table 5. Results of compatibility tests with hydrazine

Material	Sample No.	Description	Days to reach		Pressure at 200 days, psia	Total number of days in test	Pressure attained, psia	Test in process as of 3/1/67
			20 psia	35 psia				
Stainless steel	20	19-9 DL	405	1064	12	1154	37	
	19	430	172	374	22	408	39	
	22	440c	191	313	21	461	39	
	16	410	171	311	24	367	40	
	137	310	126	257	26	278	40	
	136	304L	84	205	34	239	40	
	17	416	56	103	—	119	40	
	135	304	54	97	—	110	40	
	18	420	42	91	—	108	38.5	
	134	303	35	63	—	86	41	
	183	A286	40	61	—	67	40	
Aluminum	244	356-T6	—[a]	—	0	692	3.5	Yes
	243	356-T6	—[b]	—	2	692	8.5	Yes
	184	7178	457	773	9	835	39.5	
	185	7178	335	626	12	711	41.5	
	24	6061-T6	201	421	19	506	41.5	
	186	7075-T6	89	275	30	297	42	
	187	7075-T6	276	453	—	635	43	
Miscellaneous	94	Platinum foil	—[c]		2	1398	16.5	Yes
	163	Teflon-aluminum laminate	663	1044	6	1198	42	
	23	1018 steel	133	210	30	286	39	
	90	Gold	78	119	—	166	40	
	133	6061-T6 Al (brazed)	—[d]	—	2	1317	19.5	Yes
	49	6061-T6 Al and 75-A Ti (brazed)	130	288	29	343	39	
	47	6061-T6 Al and 303 SS (brazed)	148	169	—	180	31	
	249	Vicalloy	43	85	—	100	41	
Lubricants	108	6061-T6 Al with Apiezon-L	—[e]		2	1314	15.5	Yes
	105	6061 T6 Al with Rulon	1182	—[f]	1	1314	24	Yes
	101	6061-T6 Al with Rulon	25	49	—	77	48	
	107	6 AL-4V Ti with Apiezon-L	1096	—[g]	2	1314	26	Yes
	103	6 AL-4V Ti with Rulon	254	361	14	431	42	
	106	347 SS with Apiezon-L	126	247	25	273	40	
	102	347 SS with Rulon	57	95	—	121	40	

[a] 3.5 psia at 677 days.
[b] 8 psia at 676 days.
[c] 16 psia at 1385 days.
[d] 19 psia at 1304 days.
[e] 15 psia at 1300 days.
[f] 23.5 psia at 1294 days.
[g] 25 5 psia at 1300 days.

Table 5 (contd)

Material	Sample No.	Description	Days to reach		Pressure at 200 days, psia	Total number of days in test	Pressure attained, psia	Test in process as of 3/1/67
			20 psia	35 psia				
Ceramics and lubes	40	3/8 in. ceramic ball (Al_2O_3)	482	895	9	983	40	
	49	3/8 in. ceramic ball (Al_2O_3)	326	483	17	571	40	
	51	3/8 in. ruby ball	182	397	22	449	40	
	104	Ceramic ball and Rulon	646	1059	2	1134	41.5	
	146	1/4 in. ceramic ball and moly coat	379	1030	10	1066	39	
	109	Ceramic ball and Apiezon L	259	410	13	457	40	
Butyl elastomers	194	Parker B 496-7	64	118	—	126	41	
	193	Parker B 496-7	61	118	—	126	40.5	
	195	Parker B 496-7	61	117	—	126	41.5	
	197	Parker B 480-7	47	85	—	109	40	
	198	Parker B 480-7	42	83	—	98	42.3	
	196	Parker B 480-7	41	82	—	98	42	
	122	Hadbar #XB-800-71	38	79	—	97	39	
	53	Stillman Sh 634-70	44	73	—	77	37	
	149	Stillman SR 634-70	27	47	—	56	40	
	129	Stillman SR 634-70	2	9	—	16	50	
	148	Stillman SR 613-75	17	24	—	36	58	
	61	C.H.R. #4131	35	67	—	72	38	
	57	C.H.R. #3609	32	60	—	68	40	
	147	Fargo FR 6-60-26	32	61	—	74	40	
	125	Fargo FR 6-60-26	<1	10	—	26	48	
	55	Fargo FR 6-60-27	19	44	—	49	38	
EPR elastomers	155	Parker E 515-8	—[h]	—	4	231	17	Yes
	15	Parker E 515-8	—[i]	—	—	89	12	
	200	Parker E 529-6	367	689	12	842	43	
	201	Parker E 529-6	325	650	12	742	41	
	199	Parker E 529-6	262	528	15	613	42	
	162	Stillman SR EX 983S-75	198	389	20	476	40	
	160	Stillman SR EX 983S-75	119	297	24	317	37	
	164	Stillman SR 722-70	112	165	—	175	40	
	165	Stillman SR 722-70	107	161	—	175	40	
	168	Stillman SR 722-70	31	53	—	71	46	
	63	Stillman SR EX 1004-70	16	26	—	30	41	
	11	Thiokol 132/54	5	8	—		40	
SBR elastomers	58	C.H.R. #3818	90	200	35	309	40	
	123	C.H.R. #4610	54	198	35	239	40	
	59	C.H.R. #3906	85	—	—	492	16	
	60	C.H.R. #3954	64	114	—	124	40	
	124	C.H.R. #4762	36	67	—	97	42	
Miscellaneous elastomers	157	G.E. RTV-60 (Silicon)	189	296	21	359	40	
	62	C.H.R. #4706 (PBR)	21	42	—	49	39	
	156	DuPont 5109D-590 (EPTR)	3	7	—	8	42.5	
Butyl bonded to 6-4 titanium strips	120	Stillman SR 634-70	68	208	33	240	40	
	121	Stillman SR 634-70	52	133	—	180	31	
	119	Stillman SR 634-70	52	121	—	180	40	
	118	Stillman SR 634-70	52	121	—	155	40	
	171	Hadbar XB-800-71	45	74	—	86	40	
	170	Hadbar XB-800-71	45	74	—	86	40	
	169	Hadbar XB-800-71	42	67	—	86	44	

[h] 16.5 psia at 1250 days.
[i] 10 psia at 189 days.

Table 5 (contd)

Material	Sample No	Description	Days to reach		Pressure at 200 days, psia	Total number of days in test	Pressure attained, psia	Test in process as of 3/1/67
			20 psia	35 psia				
[illegible] bonded to 4 titanium strips	203	Parker E-529-6	274	531	15	608	41	
	204	Parker E-529-6	200	377	20	541	43	
	182	Parker E-515-8	211	528	19	770	41	
	175	Stillman SR 722-70	93	259	32	322	40	
	177	Stillman SR 722-70	91	239	33	339	40	
	176	Stillman SR 722-70	84	182	38	283	43	
	174	Hadbar EPR 500-2	50	88	—	115	42	
	172	Hadbar EPR 500-2	47	88	—	108	42	
	173	Hadbar EPR 500-2	43	78	—	97	42	
N_2H_4 only	245	Control sample — blank	—[j]	—	2	692	7	
	179	Control sample — blank	—[k]	—	4	800	8.5	
	138	Control sample — blank	1188	—[l]	3	1317	22.5	Yes
	206	Control sample — blank	597	786	5	854	39.5	Yes
	145	Control sample — blank	532	1101	9	1208	42	
	158	Control sample — blank	590	1012	6	1137	42	
	205	Control sample — blank	408	677	9	741	41	
	178	Control sample — blank	326	566	15	642	41	
	189	Control sample — blank	172	337	22	433	45	
	207	Control sample — blank	86	139	—	180	40	
	130	Control sample — blank	66	220	34	277	40	
	126	Control sample — blank	44	84	—	86	40	

[j] 7 psia at 676 days.
[k] 8.5 psia at 800 days.
[l] 22 psia at 1303 days.

Table 6. Results of compatibility tests with hydrazine/hydrazine nitrate mix (75% N_2H_4, 24% $N_2H_5NO_3$, 1% H_2O)

Material	Sample No.	Description	Days to reach		Pressure at 200 days, psia	Total number of days in test	Pressure attained, psia	Test in process as of 3/1/67
			20 psia	35 psia				
Stainless steel	143	310	301	686	13	809	40	
	231	310	250	568	16	666	45	
	232	310	200	539	20	606	40	
	142	304L	194	322	20	350	39.5	
	236	304L	127	251	28	319	43	
	235	304L	64	149	—	191	43	
	233	347	51	120	—	129	40	
	234	347	46	108	—	134	44	
	95	347	48	104	—	118	40	
	45	347	26	49	—	55	40	
	141	304	264	425	15	541	40	
	230	304	41	57	—	70	40	
	97	304	31	45	—	48	38	
	229	304	14	40	—	42	40	
	96	303	29	46	—	49	37	
	227	303	10	16	—	17	45	
	228	303	10	13	—	17	44	
	41	416	12	18	—	29	54	

Table 6 (contd)

Material	Sample No.	Description	Days to reach		Pressure at 200 days, psia	Total number of days in test	Pressure attained, psia	Test in process as of 3/1/67
			20 psia	35 psia				
Titanium	212	6Al-4V Ti	—[a]	—	4	832	13	Yes
	213	6Al-4V Ti with 6061-T6 Al	—[b]	—	3	832	9	Yes
	214	6Al-4V Ti with 321 SS	194	414	16	594	40	
	209	6Al-4V-ELI Ti	—[c]	—	3	832	8	Yes
	210	6Al-4V-ELI Ti with 6061-T6 Al	—[d]	—	3	832	8.5	Yes
	211	6Al-4V-ELI Ti with 321 SS	237	561	21	572	44	
	215	5Al-2.5 Sn Ti	761	—[k]	5	832	23	Yes
	216	5Al-2.5 Sn Ti with 6061-T6 Al	594	—[l]	7	832	31	Yes
	217	5Al-2.5 Sn Ti with 321 SS	213	531	19	596	41.5	
	218	5Al-2.5 Sn-ELI Ti	—[e]	—	2	832	7.5	Yes
	219	5Al-2.5 Sn-ELI Ti with 6061-T6 Al	—[f]	—	3	832	15	Yes
	220	5Al-2.5 Sn-ELI Ti with 321 SS	215	485	19	586	40	
	221	6Al-6V-2 Sn Ti (annealed)	—[g]	—	3	832	9	
	222	6Al-6V-2 Sn Ti with 6061-T6 Al	—[h]	—	2	832	5	Yes
	223	6Al-6V-2 Sn Ti with 321 SS	256	589	17	657	44	Yes
	224	6Al-6V-2 Sn Ti (heat treated)	—[i]	—	1	832	9	Yes
	225	6Al-6V-2 Sn Ti with 6061-T6 Al	—[j]	—	3	832	11	Yes
	226	6Al-6V-2 Sn Ti with 321 SS	219	495	19	586	40	
	46	6Al-4V Ti	91	138	—	158	41	
Aluminum	43	6061 T6 Al	—[m]	—	5	1413	19	Yes
	237	6061-T6 Al	734	—[t]	6	779	21	Yes
	42	6061-T6 Al	783	1437	9	1413	35	Yes
	238	6061-T6 Al	116	163	—	191	44	
	139	6061-T6 Al (brazed)	—[n]	—	3	1317	17.5	Yes
	100	6061-T6 Al (sprayed with Rulon)	405	843	10	1030	40	
Miscellaneous metals	99	6061-T6 Al brazed to 304 SS	20	33	—	34	37	
	98	6061-T6 Al brazed to 303 SS	14	25	—	28	40	
	250	Vicalloy	8	11	—	12	42	
	52	⅜ in. ceramic ball, Al_2O_3	91	173	—	190	38.5	
	44	Ni—Span—C	12	20	—	29	52	
	50	⅜ in. sapphire ball	138	340	27.5	383	41	
Butyl elastomers	65	FR 6-60-26 (Fargo)	23	267	30	336	40	
	127	FR 6-60-26 (Fargo)	14	34	—	39	40	
	64	FR 6-50-3 (Fargo)	68	119	—	151	45	
	131	SR 634-70 (Stillman)	12	26	—	31	43	
Fuel mix only	151	Control sample — blank	—[o]	—	2	1265	7.5	Yes
	152	Control sample — blank	—[p]	—	2	1265	5.5	Yes
	153	Control sample — blank	—[q]	—	2	1265	12.5	Yes
	154	Control sample — blank	—[r]	—	2	1265	5.5	Yes
	239	Control sample — blank	—[s]	—	4	779	15	Yes
	144	Control sample — blank	766	1255	8	1317	37.5	Yes
	241	Control sample — blank	520	—[u]	11	779	35	Yes
	240	Control sample — blank	408	606	11	668	40	
	128	Control sample — blank	31	54	—	86	48	
	132	Control sample — blank	20	54	—	86	44	

[a] 13 psia at 828 days.
[b] 9 psia at 821 days.
[c] 7.5 psia at 820 days.
[d] 8 psia at 820 days.
[e] 7 psia at 820 days.
[f] 14.5 psia at 820 days.
[g] 9 psia at 820 days.
[h] 5 psia at 821 days.
[i] 9 psia at 820 days.
[j] 11 psia at 820 days.
[k] 22 psia at 820 days.
[l] 30.5 psia at 820 days.
[m] 18.5 psia at 1436 days.
[n] 17 psia at 1304 days.
[o] 7.5 psia at 1250 days.
[p] 5 psia at 1250 days.
[q] 12 psia at 1250 days.
[r] 5.5 psia at 1250 days.
[s] 15 psia at 769 days.
[t] 21 psia at 769 days.
[u] 34 psia at 769 days.

3. Bladder Development, O. F. Keller

a. Heat sterilization compatibility of EPR in hydrazine. A description of the heat sterilization compatibility test set-up, test equipment, and some preliminary heat-sterilization compatibility data are included in Ref. 1.

The first, or exploratory, phase of the heat-sterilization compatibility program now has been completed. Table 7 is a revised compilation of heat sterilization test histories. Container no. 1 was removed from the environmental test chamber after Op. 2 (operation 2), container no. 2 after Op. 4, container 3 after Op. 5, container 4 after Op. 6, container 5 after Op. 7, and container 6 after Op. 9. The durations of heat soak shown in Table 7 are accumulative (i.e., samples removed after a given test operation have also been exposed to the heat soak durations listed for all previous test operations). Table 8 provides a more complete compilation of heat-sterilization test data.

Fig. 3 represents the container pressure ranges for Op. 1 through Op. 9. Fig. 4 shows the sensitivity of the pressure generation rate to changes in test temperature.

Upon completion of Op. 9 and removal of container 6 from the environmental test chamber, the original amount of hydrazine placed in container 3 had been reduced by a factor of one-half. It is likely that a relatively large percentage of the missing hydrazine was vented between Op. 8 and Op. 9 when an attempt was made to "zero" the pressure transducer. Moreover, the relatively small changes in weight and shore hardness of the patch-test samples indicate that decomposition of the hydrazine rather than degradation of the EPR patch-test samples account for the greatest loss. Decomposition is further

Table 7. Ethylene propylene patch-test samples[a] heat-sterilization test histories

Test operation	Duration of heat-soak, hr	Heat-soak temperature, °F	Initial container pressure, psig	Final container pressure, psig	dP/dt (psi/hr)
Op. 1	1.33	300	50	72	16.5
Op. 2	60	170	26	31	0.083
Op. 3	24	235	40	58	0.750
Op. 4	71	235	37	94	0.803
Op. 5	9	300	50	142	10.2
Op. 6	28.50	300	47	302	8.95
Op. 7	88.25	300	55	708	7.41
Op. 8	164.50	300	40	1382	8.16
Op. 9	45	300	1252	1604	7.82

[a]Stillman Compound No. SR 722-70.

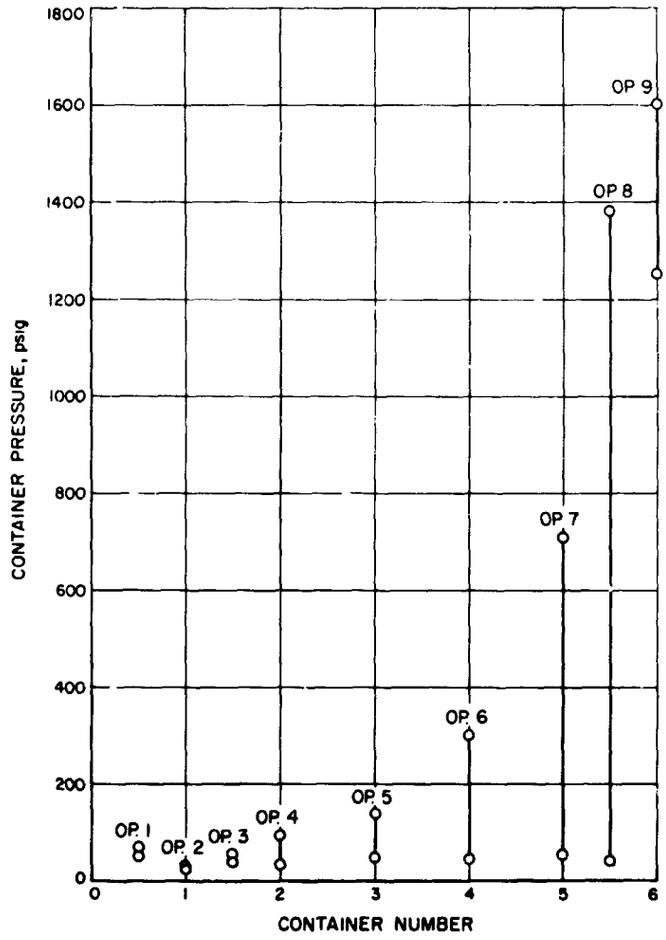

Fig. 3. Operating pressure ranges in test containers

indicated by Fig. 5, which shows changes of hydrazine concentration in the various containers after removal of each container from the environmental test chamber.

At the start of the test, the hydrazine had been colorless. When container 1 was removed from the environmental test chamber following Op. 2, the hydrazine was light brown in color, but still translucent.

The permeability data shown in Table 8 indicate inconsistency for patch-test samples removed from containers 2 and 5. Permeability tests of these samples now have been re-run. The revised permeability data are indicated in a separate column of Table 8.

Patch-test samples removed from container 6 after Op. 9 were changed very little in physical appearance, an indication that this material has excellent potential for use as an effective hydrazine bladder.

Table 8. Ethylene propylene patch-test samples heat-sterilization test data

Item	Sample No.	Thickness, in.	Initial weight, g	Final weight, g	Net increase (−decrease)	% increase (−decrease)	Permeation, Mg N_2H_4 per hr per in.^{2}	Permeation, Mg N_2H_4 per hr per in.^{2} (re-run)	Initial shore hardness A ±2.0	Final shore hardness A ±2.0	N_2H_4 color	N_2H_4 concentration, %	Samples removed following	Compound No.	Container No.
1	66 × 09200-1-a_1	0.037/0.038	1.3635	1.3662	0.0027	0.20	0.030	—	70.0	69.5	None	98.8	Op. 2	SR722-70	1
2	-1-a_2	0.035/0.036	1.2930	1.2975	0.0045	0.35	0.030	—	70.0	69.5		—			
3	-1-b_1	0.037/0.041	3.4570	3.4798	0.0228	0.66	0.020	—	69.5	69.5		—			
4	-1-b_2	0.039/0.042	3.1698	3.1822	0.0124	0.39	0.040	—	71.5	69.5		—			
5	-2-a_1	0.035/0.038	1.3550	1.3608	0.0058	0.43	0.002	0.040	72.0	69.0	Light brown	98.6	Op. 4		2
6	-2-a_2	0.036/0.038	1.3084	1.3170	0.0086	0.66	0.001	0.039	70.5	69.0		—			
7	-2-b_1	0.037/0.039	3.2670	3.2820	0.0150	0.46	0.001	0.045	67.5	69.0		—			
8	-2-b_2	0.040/0.043	3.4814	3.5037	0.0223	0.64	0.002	0.033	65.5	69.0		—			
9	-3-a_1	0.037/0.038	1.3420	1.3582	0.0162	1.21	0.030	—	71.5	67.0		98.4	Op. 5		3
10	-3-a_2	0.033/0.034	1.2184	1.2338	0.0154	1.27	0.010	—	72.0	70.0		—			
11	-3-b_1	0.040/0.043	3.4260	3.4638	0.0378	1.10	0.020	—	71.5	68.0		—			
12	-3-b_2	0.040/0.042	3.4193	3.4590	0.0397	1.16	0.002	—	65.5	69.0		—			
13	-4-a_1	0.035/0.037	1.3033	1.3007	(−0.0026)	(−0.20)	0.034	—	72.5	71.0		97.6	Op. 6		
14	-4-a_2	0.034/0.036	1.2904	1.2876	(−0.0028)	(−0.22)	0.035	—	73.0	70.0		—			
15	-4-b_1	0.035/0.038	3.2336	3.2332	(−0.0004)	(−0.01)	—	—	66.5	72.0		—			
16	-4-b_2	0.038/0.041	3.2397	3.2391	(−0.0006)	(−0.02)	—	—	67.0	68.0		—			
17	-5-a_1	0.037/0.039	1.3396	1.3529	0.0133	0.99	0.130	0.046	71.5	69.0		96.7	Op. 7		5
18	-5-a_2	0.032/0.035	1.2083	1.2183	0.0100	0.83	0.160	0.042	72.5	69.0		—			
19	-5-b_1	0.041/0.044	3.5659	3.6000	0.0341	0.96	—	—	69.5	68.0		—			
20	-5-b_2	0.039/0.043	3.4633	3.4924	0.0291	0.84	—	—	69.5	68.0		—			
21	-6-a_1	0.033/0.035	1.2372	1.2361	(−0.0011)	(−0.09)	0.036	—	71.5	73.0		95.1	Op. 9		6
22	-6-a_2	0.037/0.040	1.4035	1.4061	(−0.0024)	(−0.17)	0.026	—	71.0	70.0		—			
23	-6-b_1	0.035/0.039	3.2000	3.1956	(−0.0044)	(−0.14)	—	—	72.5	74.0		—			
24	-6-b_2	0.042/0.045	3.4977	3.4944	(−0.0033)	(−0.09)	—	—	73.0	70.0		93.7			

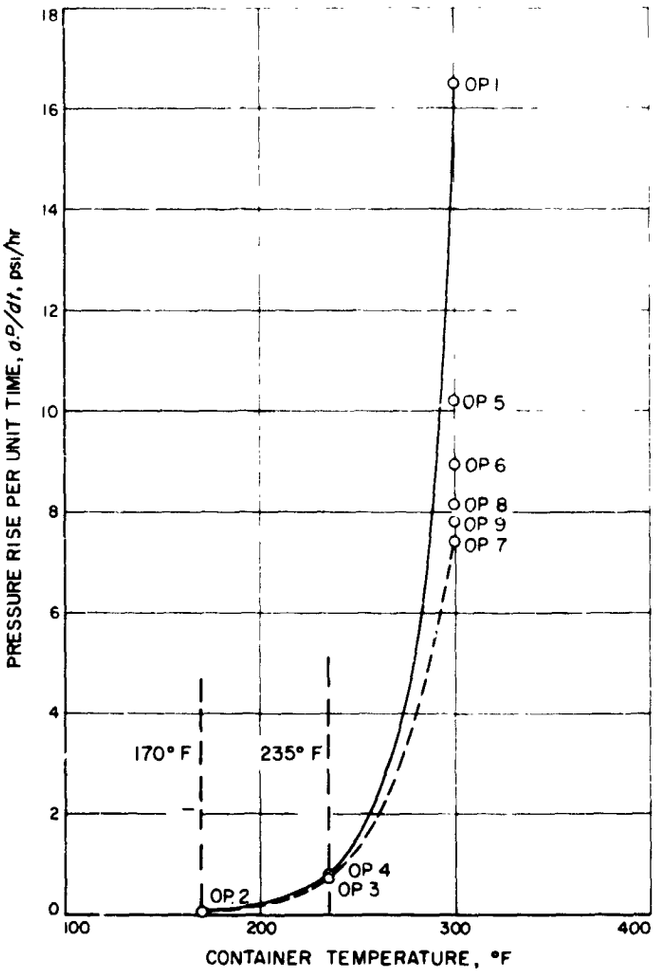

Fig. 4. Temperature sensitivity of EPR patch-test samples in N_2H_4

b. Stability of hydrazine. During previous glass vial testing with elastomers in hydrazine (Ref. 3), large quantities of NH_3, nitrogen, and hydrogen were present. The equation,

$$3N_2H_4 \rightarrow 2NH_3 + 2N_2 + 3H_2$$

might reasonably approximate the chemical breakdown of hydrazine. Substituted hydrazines such as MMH (monomethylhydrazine) are more stable than N_2H_4.

C. Injector Development: Impinging Sheet Injectors, *R. W. Riebling*

Introduction

A jet of liquid from a round orifice directed tangentially against a solid, concave deflector surface spreads to form

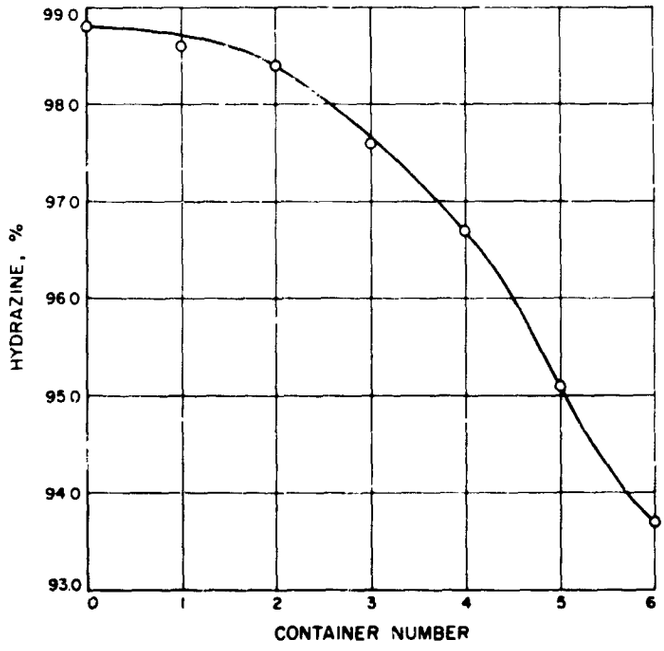

Fig. 5. Final hydrazine concentration in test containers

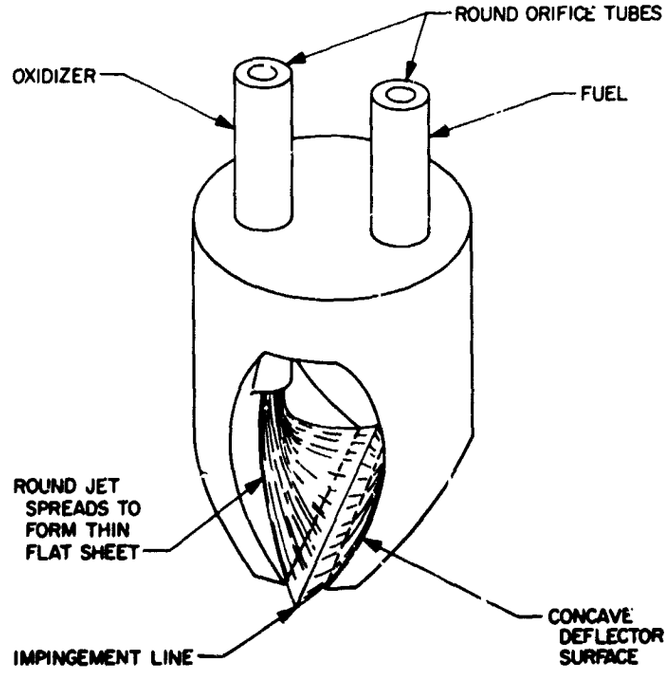

Fig. 6. Typical impinging-sheet injector element

a planar (typically, 0.005-0.010 in. thick) flowing sheet. A number of novel injector elements can be built around this sheet formation process; one of these, known as the impinging-sheet element, is shown in Fig. 6. In this

element, flat sheets of fuel and oxidizer are formed separately, then brought together along an impingement line. Impinging-sheet injectors have been under development at the Jet Propulsion Laboratory for some time. Early work by Evans (SPS 37-34, Vol. IV, p. 174, and SPS 37-35, Vol. IV, p. 152), produced design criteria for single impinging-sheet elements with the nitrogen tetroxide (N_2O_4) hydrazine (N_2H_4) propellant combination at a mixture ratio of 1.2. The work was done at the 25-lb_f-thrust-per-element level. These criteria were applied directly to the design of a multiple-element, 2000-lb_f-thrust, impinging-sheet injector that was operated at the same mixture ratio, the same level of thrust-per-element, and with the same propellant combination. The results demonstrated that impinging-sheet injectors exhibit a number of distinct advantages over the more conventional types. Some of these advantages are:

(1) Relative insensitivity of performance to manufacturing tolerances.

(2) Superior performance levels (measured as characteristic exhaust velocity c^* in ft/sec).

(3) Wide throttling capability using several different throttling techniques without appreciable degradation in characteristic velocity efficiency, η_{c^*}.

(4) Extremely smooth and stable combustion.

Because of these inherent advantages, the impinging-sheet injection concept seems particularly well suited for a wide variety of other propellant combinations (especially the high-energy, space-storables) over a broad spectrum of space mission profiles. The principles of sheet formation, and the relationships governing the combination of sheets into injection elements are discussed in Refs. 4 and 5, respectively.

To extend this promising new injection technique to other applications, some additional design criteria are required. One area of particular interest is the protection of impinging-sheet elements during throttled operation when they are shut off and exposed to the extreme convective heat transfer environment without cooling by the normally-present flow of propellants along the deflectors. The multiple-element, 2000-lb_f-thrust injector mentioned previously had elements mounted externally to the injector face; some of these elements were severely eroded when not cooled by propellant flow (Fig. 7). One possible remedy is to recess the elements within the injector face to reduce convective heat transfer and provide greater opportunity for conduction of heat away from shut-off elements and into the body of the injector.

Another area of interest concerns the feasibility of scaling up the present designs to higher levels of thrust-per-element. Both the mixing and the atomization of a pair of impinging *jets* of unlike propellants are severely impaired as the jet diameters are increased (SPS 37-36, Vol. IV, p. 174), which results in degraded performance. It must be learned whether unlike impinging *sheets* are subject to the same critical limitations.

To investigate both areas simultaneously, a 100-lb_f thrust unlike impinging-sheet single element was designed, fabricated, and test-fired with N_2O_4, N_2H_4. Auxiliary attachments permitted controlled variation of the element's external geometry to include the simulation of a fully recessed installation. The effects of several different external configurations on performance were measured, and a way was found to bury the impinging-sheet elements within the face of an injector without an appreciable decrease in performance below that obtained when elements are mounted in a fully-external position. However, the c^* efficiency level of the 100-lb_f-thrust, single element was only about 85% (in both the external and the recessed positions). Because the earlier 25-lb_f elements were about 95% efficient, these results indicated that the performance of impinging-sheet elements is degraded as their physical size is increased. A series of experiments was then conducted in an attempt to understand more fully the nature of this phenomenon. This report will present and discuss the results of this investigation.

2. Apparatus

The basic 100-lb_f impinging-sheet injector element is illustrated in Fig. 8. In the geometry of its orifices and internal deflector surfaces, this injector was a scaled-up version of the earlier, 25-lb_f element. It was designed not only for equal fuel and oxidizer pressure drops, but also with a momentum ratio of unity, thus fulfilling the optimum mixing requirements for a pair of impinging streams of unlike liquids (Ref. 6).

Two identical stainless steel deflector/orifice combinations were mounted to the face of the injector so that the spacing between their knife-edges could be varied continuously between zero and 0.1 in. Each orifice had a 0.075-in. diameter, and a 100-diameter length to insure fully-developed turbulent flow with its reproducible hydraulic characteristics. The jet of liquid emerging from each orifice was introduced tangentially to a concave deflector surface of 0.58-in. radius, where it spread to form a thin, flat sheet. After being turned through angles of 45 deg on the deflectors, the sheets (one of fuel, the

(a) WITH PROPELLANT FLOW (b) WITHOUT PROPELLANT FLOW

Fig. 7. Steel impinging-sheet injector element after throttled firing: (a) cooled by propellant flow, (b) without propellant flow

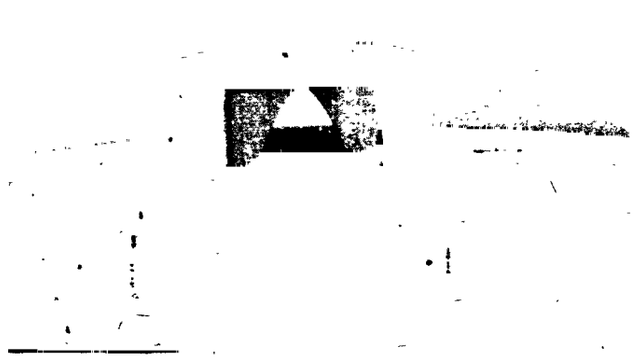

Fig. 8. Basic impinging-sheet injector element

Fig. 9. Impinging-sheet element enclosed by unvented sides

other of oxidizer) impinged at 90 deg to form a finely divided spray.

To study the effects of burying this element within the face of an injector, a set of "sides" was made, which, when clamped in place around the basic element (Fig. 9) completely enclosed the sheet formation devices. The only egress for the propellants was through the narrow slit between the two deflectors.

When similar impinging-sheet elements are flowed with inert propellant simulants, a small but not negligible amount of backspray emanates from the impingement line (Fig. 10). If such a backspray forms with the reactive propellants, some combustion might take place within the cavity between the two deflectors. This has caused no problems where the cavity is open to the surrounding chamber environment, as in the external installations shown in Fig. 8, but with the cavity completely enclosed as in Fig. 9, any gases produced by a reactive backspray could exit only through the slot between the deflectors. If this action interfered with the proper impingement of the propellant sheets, less efficient combustion could result. Accordingly, a second set of sides was fabricated, identical to the first except for vent passages designed to offer the least resistance to the escape of any backspray combustion products formed. These sides are shown in Fig. 11.

Fig. 10. Edge view of impinging liquid sheets showing backspray

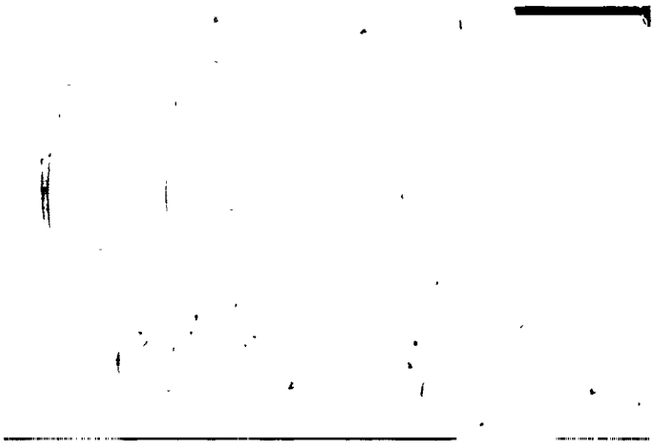

Fig. 11. Impinging-sheet element enclosed with vented sides

To determine the effect on performance of recirculation patterns in the vicinity of the impingement region the external surfaces of both deflectors were cut back, as shown in Fig. 12, a top view. This made the element similar to the 25-lb$_f$ elements (Fig. 7) in external, as well as internal geometry.

The final configuration (Fig. 13, which also shows the cutback external deflector surfaces of Fig. 12) included an insert that considerably reduced the volume of the

Fig. 12. Impinging-sheet element with deflector sides cut back

Fig. 13. Impinging-sheet element with sides removed to show insert between deflectors

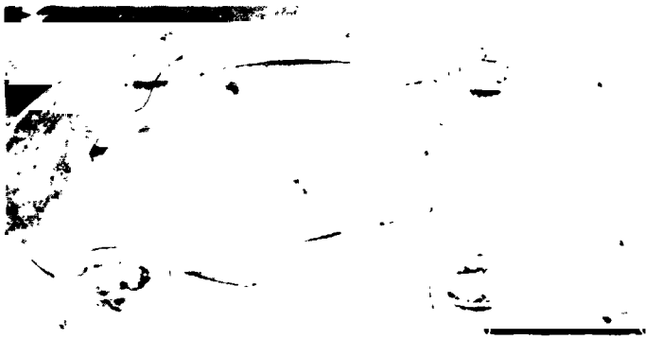

Fig. 14. Impinging-sheet element with unvented sides

cavity between the deflectors without interfering with the sheet-formation process. The element containing this insert was enclosed with a set of unvented sides (Fig. 14).

All of the injector configurations described above were fired in an uncooled, steel thrust chamber under ambient conditions 13.5 psia. Table 9 summarizes the chamber geometry. In addition, the injector configuration shown in Fig. 12 was fired into a baffled chamber during a series of stream-separation experiments discussed later in this report. The baffled chamber was described in detail in SPS 37-31, Vol. IV, p. 192. It was similar to the chamber of Table 9, except for its greater characteristic chamber length L^* of 50 in., and the baffle and side spray apparatus customarily used in stream-separation firings.

Table 9. Summary of the 100-lb$_f$ thrust chamber geometry

Measurement	Value
Cylindrical length[a]	4.4 in.
Diameter	2.0 in.
Throat area	0.5458 in.^{2}
Characteristic length[a]	28.6 in.
Expansion area ratio	2.134
Convergence half angle	40 deg
Divergence half angle	15 deg

[a]With injector and accessories installed.

3. Results and Discussion

Eight short-duration firings of 1 to 3 sec each were conducted to assess the effects of external element geometry on the performance of the 100-lb$_f$ impinging-sheet injector. The propellants were N_2O_4/N_2H_4 at a nominal mixture ratio of 1.25, and chamber pressures that ranged between approximately 100 and 120 psia. The results are summarized in Table 10. Chamber pressures were measured at the entrance to the convergent section of the nozzle and corrected to stagnation values. The spacing between the two deflectors was constant at 0.05 in., except in Tests 6 and 7, where it was intentionally varied. Characteristic velocity efficiency (η_{c^*}), expressed in percent, was chosen as the comparative index of performance level, and is the ratio of the measured value of c^* to that theoretically attainable with full shifting equilibrium flow at the experimentally measured values of chamber pressure and mixture ratio. No corrections were made to the measured values of c^* because the results were to be used primarily for comparative purposes.

The results are presented in graphical form in Figs. 15 through 18. Where the basic injector configuration of

Table 10. The effects of external element geometry on performance of 100-lb$_f$ impinging-sheet injector

Test No.	Injector configuration	Deflector spacing, in.	Chamber pressure (p_c), psia	Total flow rate ($\dot{w}_t$), lb$_m$/sec	Mixture ratio (r)	Characteristic velocity (c^*), ft/sec	Efficiency (η_{c^*}), %
1	Basic external installation (Fig. 8)	0.05	115	0.407	1.25	5090	87.7
2	Element enclosed with unvented sides (Fig. 9)	0.05	98	0.430	1.25	4010	69.5
3	Same as test no. 2	0.05	99	0.422	1.22	4130	71.2
4	Element enclosed with vented sides (Fig. 11)	0.05	113	0.416	1.27	4780	82.5
5	External surfaces of deflectors cut back, no sides (Fig. 12)	0.05	118	0.416	1.24	5000	86.4
6	Same as test no. 5	0.075	114	0.416	1.24	4830	83.4
7	Same as test no. 5	0.10	116	0.414	1.24	4920	84.9
8	Element enclosed with unvented sides and insert between deflectors (Fig. 14)	0.10	99	0.422	1.23	4130	71.3

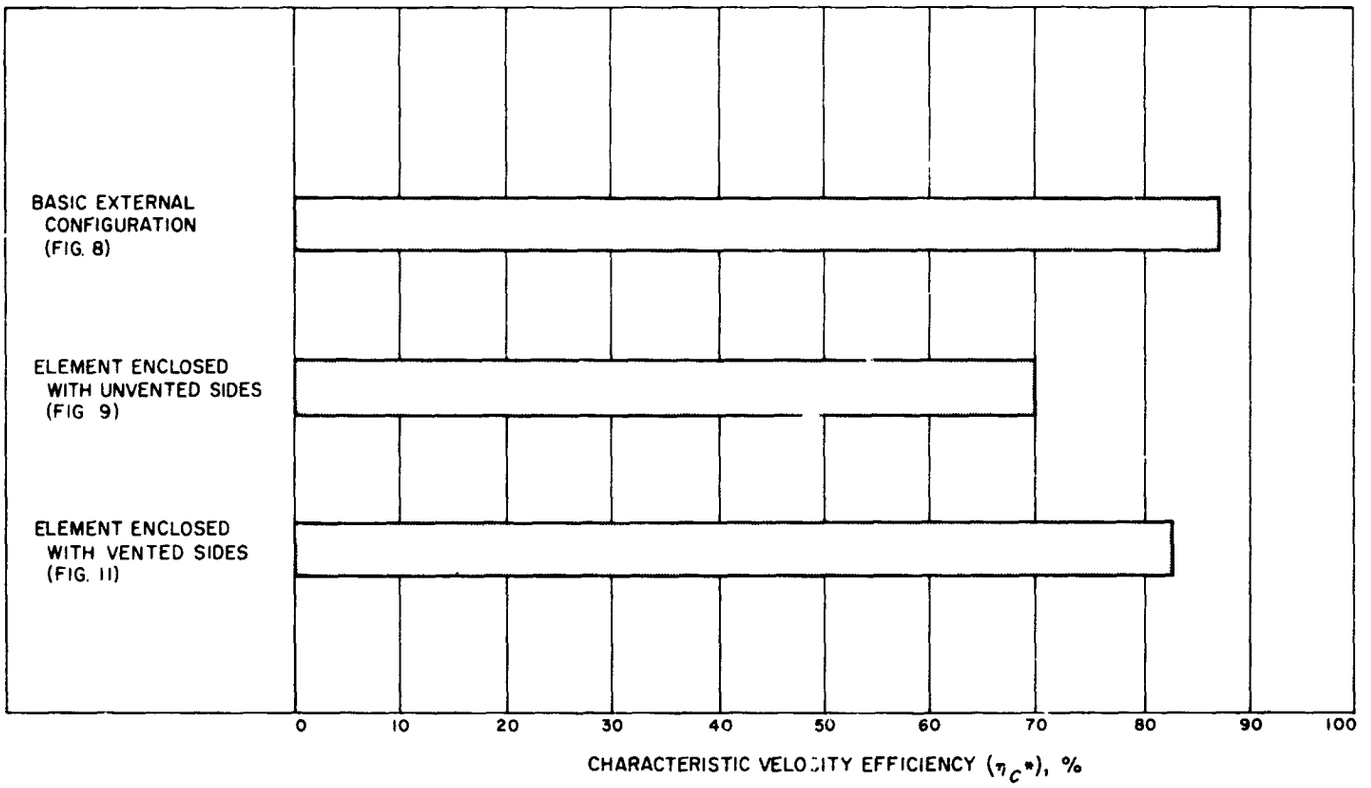

Fig. 15. The effect of side venting on performance of impinging-sheet injector (0.05-in. deflector spacing)

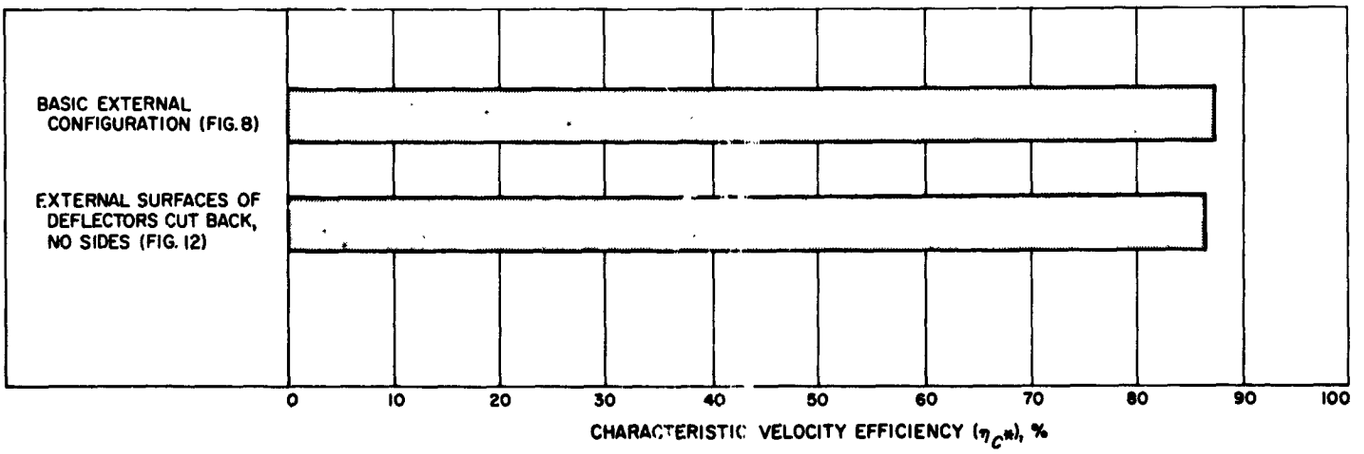

Fig. 16. The effect of external deflector geometry on performance of impinging-sheet injector (0.05-in. deflector spacing)

Fig. 8, which represents the typical external installation, was enclosed by sides (Fig. 9) simulating fully-recessed mounting, its performance index (η_{c*}) dropped from 87.7% to only 69.5% (Fig. 15). Yet when those sides were provided with vent passages, each with a cross-sectional area that was large relative to the area of the slot between the deflectors, η_{c*} was restored to nearly its original value. No attempt was made to optimize the area or the contours of the vent passages in this brief program, but it seems reasonable that suitably-designed vents with fully buried elements would give the same performance as vents with completely exposed elements.

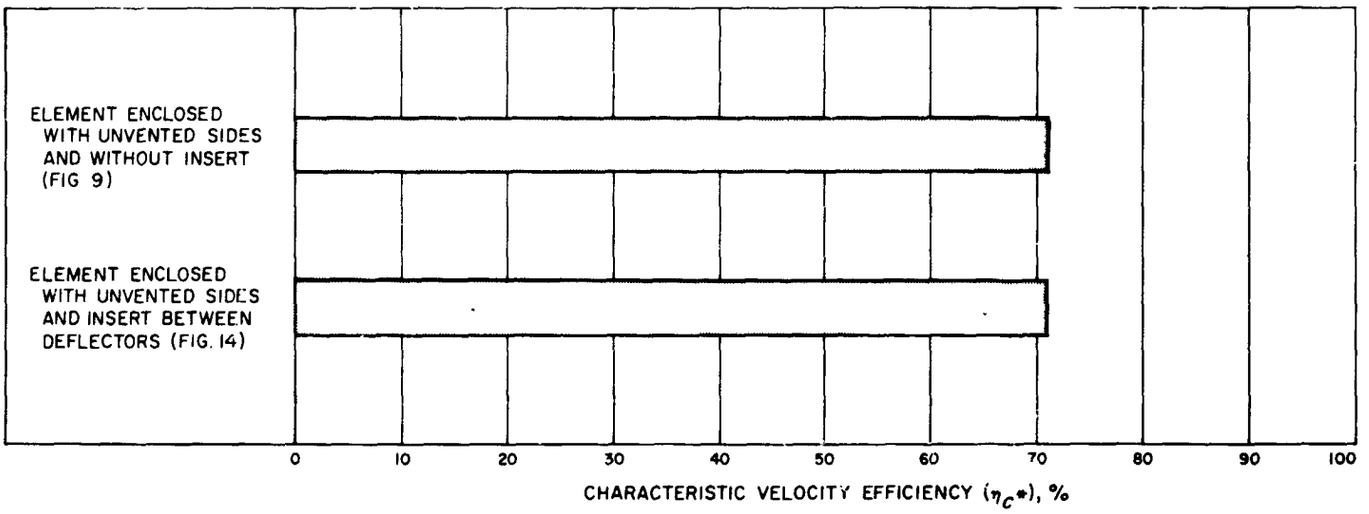

Fig. 17. The effect of internal cavity volume on performance of impinging-sheet injector (0.05-in. deflector spacing)

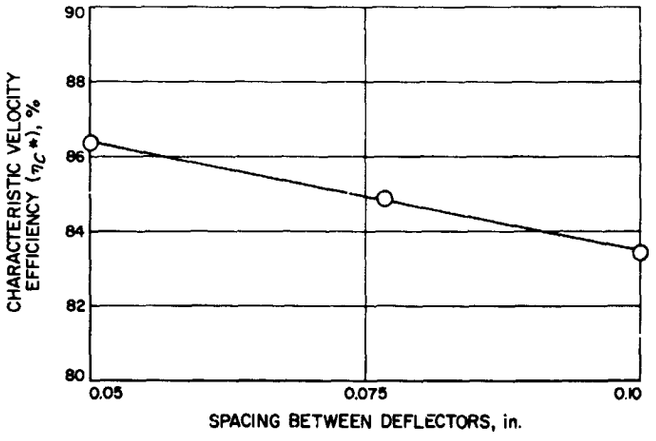

Fig. 18. The effect of deflector spacing on performance of impinging-sheet injector (the configuration of Fig. 12)

Fig. 16 indicates no change in performance with the external surfaces of the deflectors in Fig. 3 cut back to give the configuration of Fig. 7. If gas recirculation patterns had been present in the vicinity of the deflector knife-edges, they would have been debilitated by the geometery of Fig. 3 and enhanced by that of Fig. 7. Because the performance of both configurations is nearly identical, gas recirculation is either absent or does not play a significant role in the operation of the impinging-sheet injection element. Furthermore, the data in Fig. 16 indicate that a properly-vented element buried flush with the face of an injector should perform as well as one of the same scale that has cutback deflectors and is mounted externally. The degradation in performance of buried elements without vents is not fully understood at this time, but may be the result of sheet disruption by gases from a reactive backspray discussed earlier.

To facilitate machining, the deflectors of impinging-sheet injectors are made usually with full internal radii, as shown in Fig. 8, although only a small portion of the resulting internal surface is actually used for sheet formation. This geometry results in a relatively large cavity between the deflectors. The solid insert (Fig. 13) reduced the volume of this cavity by about 75%, leaving only sufficient clearance for sheet formation, yet a buried, unvented element with this reduced cavity volume (Fig. 14) gave the same performance as a buried, unvented element with the full internal volume (Fig. 17). This would suggest that whatever performance degradation exists with buried, unvented elements is not greatly influenced by the internal cavity volume.

The effect of deflector spacing on performance is shown in Fig. 18; at least over the range of spacings investigated, closer spacing results in higher performance. This is in agreement with the earlier 25-lb_f, single element results reported in SPS 37-34, Vol. IV, p. 174, and in SPS 37-35, Vol. IV, p. 152. It is substantiated also by recent cold flow studies at JPL, the subject of a future SPS article, which have shown that deflector spacing exerts a major influence on the mixing efficiency of unlike-impinging sheets. Closer spacings result in higher values of the propellant distribution index (η_M), measured in percent. Of course, lower performance might be expected from extremely close spacings that interfere with the sheets themselves. This apparently did not take place in

firings at the 0.05-in. spacing because performance steadily decreased as the spacing increased to 0.1 in.

Some of the hardware modifications investigated were capable of delivering about the same performance as the baseline design, which was the externally-mounted element. However, none of these modifications to the basic concept resulted in improved performance, and, with this 100-lb_f impinging-sheet injector, it seems that 85 or 88% is an effective upper limit to the c^* efficiencies attainable in chambers with characteristic lengths of about 30 in. If this is true, the performance of impinging-sheet injectors decreases as their physical size increases, behavior that is similar to that of conventional impinging-jet injectors.

For most propellant combinations, regardless of the type of injector used, these primary processes must take place to ensure efficient combustion: (1) propellant mixing, (2) atomization and vaporization, and (3) chemical reaction. Normally, chemical reaction rates are quite rapid compared to the rates of mixing and atomization, so that one or both of the two physical processes usually controls the overall combustion rate. For impinging-*jet* injectors, which are generically similar to impinging-sheet injectors, propellant mixing is impaired as the diameters of the impinging streams are increased. The now classical experiments of Johnson (Ref. 7) and Stanford (SPS 37-31, Vol. IV and SPS 37-36, Vol. IV) showed that impinging jets of hypergolic, highly-reactive propellants such as N_2O_4/N_2H_4 tend to "blow apart" before complete mixing in the liquid-phase because of rapid chemical reactions at the impingement interface. Although these stream separation effects are negligible with jets of small diamter (~0.02 in.), they become noticeable at intermediate diameters (~0.065 in.), and seriously degrade performance with large (~0.25 in.) diameter jets.

To determine whether the impaired propellant mixing that resulted from combustion effects limited the performance of the 100-lb_f, impinging-*sheet* element, a series of nine baffled chamber firings was made. The injector configuration shown in Fig. 12 was fired in a chamber with a characteristic length of 50 in., and the chamber was divided into two longitudinal channels by a baffle plate. The baffle was oriented to lie in a plane perpendicular to the plane in which the injector orifices lay. The top of the baffle was situated a short distance from the injector plate to avoid interference with the impingement process, and the bottom of the baffle was a short distance upstream of the throat. Two full-cone spray nozzles were located in the chamber wall, one on each side of the baffle, and turbulence rings were mounted in the chamber, downstream of the spray nozzles. The objective of the experiment was to measure the difference in performance when the sprays from the side nozzles (one spraying fuel and the other oxidizer) were reversed.

The concept involved follows: if the propellants flowing from the main injector are repelled from each other to form a fuel-rich zone on the fuel orifice side of the chamber, and an oxidizer-rich zone on the oxidizer side, the baffle should prevent secondary mixing because of turbulence and diffusion. Thus, one channel should contain an oxidizer-rich flow, and the other a fuel-rich flow of gases. Spraying oxidizer into fuel-rich gases and fuel into the oxidizer-rich gases (termed "unlike" propellants), should increase performance, while spraying fuel into fuel-rich gases and oxidizer into oxidizer-rich gases (termed "like" propellants), should reduce performance. If the streams from the main injector do not blow apart, and a nearly uniform mixture-ratio distribution exists in the chamber, performance should remain relatively unchanged when the propellant sprays are reversed. If the streams penetrate each other, the fuel-rich and oxidizer-rich channels will be reversed, and the performance changes should indicate this condition, as well.

The apparatus and procedures were identical to those used by Stanford (SPS 37-31, Vol. IV), except for the injector, which was the present impinging-sheet model. Several series of firings were conducted in which propellants were injected through the main injector as well as the side-spray nozzles along the chamber walls. In some tests, like propellants were injected at the sides, while in other tests unlike propellants were injected. In each of these series, the side flows were varied from about 10 to nearly 30% by weight of the total flow rate, while the flow through the main element was held constant. To measure the datum performance level, the engine was fired at the design flow rate with no side injection.

The results are summarized in Table 11. Performance was calculated on the basis of the total flowrate $\dot{w}_t$ of propellants (from both the main element and the side streams) injected into the chamber. The comments and qualifications made with respect to Table 10 apply to Table 11 as well.

The results of these tests are shown in Fig. 19. For purposes of comparison, the data of Stanford (SPS 37-31, Vol. IV) for a 100-lb_f unlike impinging-jet injector fired

Table 11. Degree of stream separation of unlike impinging sheets in 100-lb_f injector fired in baffled-chamber

Test No.	Kind of side spray	Oxidizer flow, lb_m/sec		Fuel flow, lb_m/sec		Total flow rate ($\dot{w}_t$), lb_m/sec	Side flow, % by weight	Overall mixture ratio (r)	Chamber pressure (p_c), psia	Characteristic velocity (c^*), ft/sec	Efficiency (η_{c^*}), %
		Main element	Side spray	Main element	Side spray						
1	Like	0.161	0.075	0.133	0.0[illegible]	0.418	29.7	1.30	108	4350	75.5
2	Like	0.160	0.036	0.133	[illegible]035	0.369	19.2	1.17	97	4440	76.5
3	Like	0.158	0.017	0.131	0.022	0.328	11.9	1.15	95	4980	85.7
4	None	0.165	0.0	0.131	0.0	0.296	0.0	1.26	90	5140	89.0
5	Unlike	0.158	0.017	0.131	0.018	0.323	10.7	1.17	100	5240	90.2
6	Unlike	0.160	0.033	0.134	0.021	0.346	15.6	1.25	104	5110	88.3
7	Unlike	0.160	0.035	0.133	0.023	0.351	19.6	1.24	106	5040	87.0
8	Unlike	0.158	0.038	0.130	0.032	0.358	19.6	1.21	109	5130	88.5
9	Unlike	0.164	0.067	0.135	0.047	0.413	27.7	1.27	121	4940	85.4

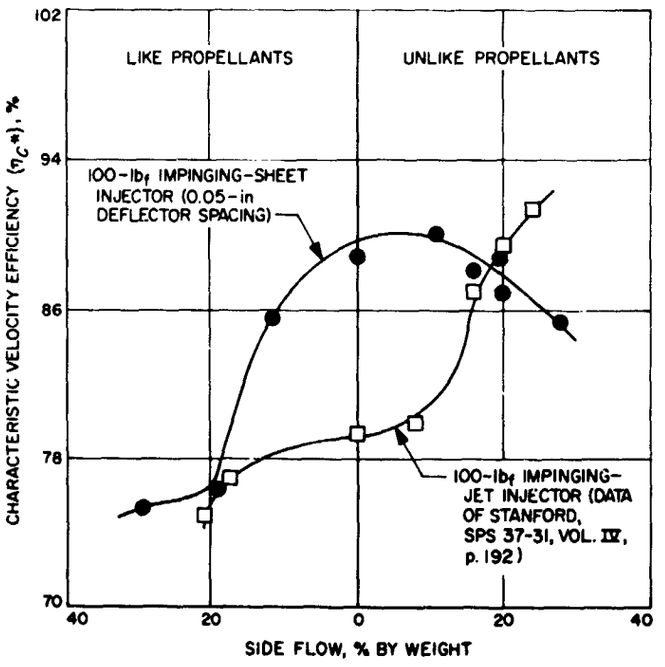

Fig. 19. Variation of c* efficiency with side flow in baffled chamber experiments using two 100-lb_f, single-element injectors

in the same apparatus[9] are included. The maximum performance ($\eta_{c^*} \cong 90\%$) with impinging sheets was realized at only about 5% unlike side flow, which indicates, at most, a very slight degree of stream separation. This performance level is slightly higher than that attained in the unbaffled chamber, probably the result of the greater L^* (50 in.) of the baffled chamber. Increasing the percentage of side flow, either like or unlike, lowered the performance, probably by the amount of heat absorbed by the uncombined propellant. Thus, for all practical purposes, the impinging sheets neither blew apart nor penetrated each other. Rather, they mixed well and produced a nearly uniform mixture ratio distribution in the chamber.

This behavior may be contrasted to that of the impinging jets, where performance increased by over twelve percentage points at maximum unlike sidespray, indicating severe blowing apart of the main element's unlike propellant streams. It would seem, then, that while rapid interfacial chemical reactions at the impingement surface interface considerably with the efficient mixing of a pair of round jets at the 100-lb_f thrust level, their effects can be virtually eliminated by transforming those streams into thin, flat sheets prior to impingement.

Because propellant mixing effects probably are not the cause of performance degradation as the physical size of impinging-sheet elements is increased, the atomization process is logically suspect. Most modern combustion models recognize the influence of propellant drop size on vaporization, and therefore on combustion. Some years ago, Ingebo (Ref. 8) studied the atomization of like impinging jets of heptane in air streams. He published an equation relating the volumetric mean droplet diameter ($\bar{D}_{sc}$, measured in microns), to the jet diameter (D_j, measured in in.), jet velocity (V_j, measured either in in./sec

[9]Stanford also studied an early version of the impinging-sheet injector, but in both its geometry and its spacing between deflectors (0.72 in.) it bore little resemblance to present designs. Accordingly, valid comparisons probably cannot be made between its performance and that of the present injector.

or ft/sec), and to the difference between the airstream and jet velocities (ΔV). That equation may be simplified to

$$\overline{D}_{30} \sim \left(\frac{D_j}{V_j}\right)^{1/2} \quad (1)$$

by assuming $\Delta V = 0$. This relationship indicates that the degree of atomization that results from the self-impingement of a pair of round jets decreases as the jet diameter increases, or as the injection velocity decreases. Although Eq. (1) applies strictly to the like impingement of heptane jets only, several attempts have been made to extend it to the *unlike* impingement of jets of other liquids. A detailed discussion of this subject is clearly beyond the scope of this report. It is sufficient to say that good correlations have been obtained between $\overline{D}_{30}$ and $(D_j/V_j)^{1/2}$ in cold flow drop-size experiments with like impinging jets of water and other liquids, and between η_{c*} and $(D_j/V_j)^{1/2}$ in test firings where atomization controlled the combustion process. The data for unlike impinging streams do not correlate quite as well, but do show the same general trend. In brief, then, the degree of atomization in the spray produced by a pair of impinging jets decreases as the diameter of the jets increases, assuming a constant injection velocity. It would not be surprising to find similar effects because of physical size in the atomization of impinging sheets. This, and the demonstrated absence of mixing effects would suggest that impinging-sheet injection elements are atomization-limited at higher levels of thrust-per-element. In general, the controlling parameter may prove to be the stream cross-sectional area rather than the diameter, which is meaningful only for round jets.

References

1. Keller, O. F., "Heat-Sterilization Compatibility of EPR in N_2H_4," *Supporting Research and Advanced Development*, Space Programs Summary 37-42, Vol. IV, p. 82. Jet Propulsion Laboratory, Pasadena, Calif., Dec. 31, 1966.
2. Vango, S. P., *Determination of Permeability of Cast Teflon Sheet to Nitrogen Tetroxide and Hydrazine*, Technical Memorandum No. 33-55. Jet Propulsion Laboratory, Pasadena, Calif., Aug. 25, 1961.
3. Weiner, R. S., "Materials Compatibility," *Supporting Research and Advanced Development*, Space Programs Summary 37-22, Vol. IV, pp. 133–134. Jet Propulsion Laboratory, Pasadena, Calif., Aug. 31, 1963.
4. Riebling, R. W., *The Formation and Properties of Liquid Sheets Suitable for Use in Rocket Engine Injectors*, Technical Report 32-1112. Jet Propulsion Laboratory, Pasadena, Calif. (to be published).
5. Riebling, R. W., "Controlling the Dimensions and Orientation of Impinging Propellant Sheets in Liquid Rocket Engine Injectors," *J. of Spacecraft and Rockets*, vol. 3, no. 11, p. 1693, Nov. 1966.
6. Rupe, J. H., *A Correlation Between the Dynamic Properties of a Pair of Impinging Streams and the Uniformity of Mixture Ratio Distribution in the Resulting Spray*, Progress Report 20-209. Jet Propulsion Laboratory, Pasadena, Calif., March 28, 1956.
7. Johnson, B. H., *An Experimental Investigation of the Effects of Combustion on the Mixing of Highly Reactive Liquid Propellants*, Technical Report 32-689. Jet Propulsion Laboratory, Pasadena, Calif., July 15, 1965.
8. Ingebo, R. D., "Drop-Size Distributions for Impinging-Jet Breakup in Airstreams Simulating the Velocity Conditions in Rocket Combusters," *Technical Note* 4222, National Advisory Committee on Aeronautics, 1958.